Earth and Planetary Science Letters 359-360 (2012) 227–239

Contents lists available at SciVerse ScienceDirect

Earth and Planetary Science Letters

journal homepage: www.elsevier.com/locate/epsl

Heterogeneous upper mantle Ne, Ar and Xe isotopic compositions and a possible Dupal noble gas signature recorded in basalts from the Southwest Indian Ridge

R. Parai [a,*], S. Mukhopadhyay [a], J.J. Standish [b]

[a] Department of Earth and Planetary Sciences, Harvard University, 20 Oxford Street, Cambridge, MA 02138, United States
[b] American Chemical Society, 1155 Sixteenth Street, N. W., Washington, DC 20036, United States

ARTICLE INFO

Article history:
Received 23 April 2012
Received in revised form
4 October 2012
Accepted 6 October 2012
Editor: B. Marty
Available online 20 November 2012

Keywords:
noble gases
Dupal
xenon
mantle heterogeneity
volatile recycling
early differentiation

ABSTRACT

Variations in heavy noble gas (Ne, Ar, Xe) isotopic compositions provide unique insights into the nature of heterogeneities in the mantle. However, few precise constraints on mantle source heavy noble gas isotopic compositions are available due to ubiquitous shallow-level atmospheric contamination. As a result, the extent of heterogeneity in mid-ocean ridge basalt (MORB) mantle source Ne, Ar and Xe isotopic compositions is unknown. Basalts from the ultra-slow spreading Southwest Indian Ridge (SWIR) between 7°E and 25°E exhibit remarkable variability in He isotopic composition: SWIR $^{4}He/^{3}He$ spans half the total range observed in all mantle-derived basalts. Therefore, basalts from the SWIR provide a unique window into upper mantle heterogeneity and present an ideal opportunity to characterize variations in upper mantle heavy noble gas isotopic composition. Here we present new high-precision Ne, Ar and Xe isotopic compositions as well as He, CO_2, Ne, Ar and Xe abundances measured in basalt glasses from the SWIR. After correcting the measured values for shallow-level atmospheric contamination, significant and systematic variations in mantle source Ne, Ar and Xe compositions are observed. We note that large variations in source $^{40}Ar/^{36}Ar$ and $^{129}Xe/^{130}Xe$ are observed in basalts removed from the influence of known hotspots, indicating a heterogeneous mid-ocean ridge basalt source. Thus, SWIR heavy noble gas data reveal a greater degree of source heterogeneity than is evident in the $^{4}He/^{3}He$ systematics alone. The observed heavy noble gas isotopic heterogeneities imply that the average MORB source $^{40}Ar/^{36}Ar$ and $^{129}Xe/^{130}Xe$ ratios are not yet well-determined.

Variation in MORB source $^{40}Ar/^{36}Ar$ and $^{129}Xe/^{130}Xe$ at a given $^{4}He/^{3}He$ and $^{21}Ne/^{22}Ne$ may reflect heterogeneous recycling of atmospheric Ar and Xe. In particular, we find low mantle source $^{40}Ar/^{36}Ar$ and $^{129}Xe/^{130}Xe$ ratios in the eastern region of the study area, which may reflect the noble gas signature of the Dupal mantle domain. Our observations require that the sampled mantle domain either is very ancient (>4.45 Ga) or has been metasomatized by subduction zone fluids carrying recycled atmospheric Ar and Xe. However, our Xe isotopic measurements indicate that differences between MORB and ocean island basalt (OIB) source noble gas compositions cannot be explained by recycling of atmospheric noble gases alone. Instead, a relatively undegassed mantle reservoir is required to account for OIB noble gases. The SWIR data demonstrate that the reservoir supplying primordial noble gases to mantle plumes differentiated from the MORB source early in Earth history, and the two reservoirs have not been homogenized over 4.45 Ga of mantle convection.

1. Introduction

Noble gases provide unique constraints on the differentiation history of the Earth. The noble gases are chemically inert and are present in very low abundances in the mantle, such that variations in mantle source noble gas isotopic composition reflect degassing, regassing and nuclear processes such as radioactive decay and spontaneous fission of more abundant parent nuclides. A full complement of noble gas analyses on mantle-derived samples provides information about volatile cycling (Holland and Ballentine, 2006; Kendrick et al., 2011; Sumino et al., 2010), mass fluxes between mantle reservoirs (e.g., Gonnermann and Mukhopadhyay, 2009; O'Nions and Tolstikhin, 1996; Porcelli and Wasserburg, 1995; Tolstikhin and Marty, 1998), budgets of the

* Corresponding author. Tel.: +1 617 384 9335.
E-mail address: parai@fas.harvard.edu (R. Parai).

0012-821X/$ - see front matter © 2012 Elsevier B.V. All rights reserved.
http://dx.doi.org/10.1016/j.epsl.2012.10.017

heat-producing elements (U, Th and K), and constraints on early Earth differentiation based on the decay products of short-lived nuclides (^{244}Pu and ^{129}I; Allègre et al., 1987; Ballentine and Holland, 2008; Caffee et al., 1999; Kunz et al., 1998; Mukhopadhyay, 2012). Therefore, precise determination of noble gas abundances and isotopes in mid-ocean ridge basalts (MORBs) and ocean island basalts (OIBs) can provide powerful insights into the history, structure and dynamics of the Earth's interior.

Mantle He and Ne isotopic compositions reflect loss due to degassing and subsequent production of select nuclides by nuclear processes, since recycling of He and Ne is thought to be insignificant (Graham, 2002; Holland and Ballentine, 2006; Porcelli and Wasserburg, 1995). ^{4}He is produced by α-decay of U and Th, while ^{3}He is primordial. As a result, high ^{4}He/^{3}He ratios are generated by degassing and subsequent ingrowth of ^{4}He, and are commonly attributed to the presence of degassed recycled material with high (U+Th)/^{3}He in the source region. In contrast, low ^{4}He/^{3}He ratios reflect a mantle source that has remained relatively undegassed and thus preserved low (U+Th)/^{3}He over time. Among Ne isotopes, ^{20}Ne and ^{22}Ne are primordial, while ^{21}Ne is produced by nuclear reactions associated with U and Th decay (^{18}O(α,n)^{21}Ne and ^{24}Mg(n,α)^{21}Ne; Yatsevich and Honda, 1997; Wetherill, 1954), such that low source ^{21}Ne/^{22}Ne ratios reflect a relatively undegassed mantle reservoir. To first order, radiogenic He should be associated with nucleogenic Ne isotopic compositions; however, mixing of mantle sources with different ^{3}He/^{22}Ne ratios may generate hyperbolic mixing arrays, complicating the expected relationship between He and Ne isotopes measured in basalts (e.g., Furi et al., 2010; Hanyu and Kaneoka, 1998; Kurz et al., 2005; Madureira et al., 2005; Moreira et al., 1995, 2011; Parai et al., 2009; Shaw et al., 2001).

Mantle Ar and Xe isotopic compositions are interpreted with respect to nuclear processes, degassing and regassing, since recycling of atmospheric Ar and Xe at subduction zones may be significant (e.g., Holland and Ballentine, 2006; Kendrick et al., 2011; Sumino et al., 2010). ^{36}Ar and ^{38}Ar are primordial, while ^{40}Ar is produced by decay of ^{40}K by electron capture. Among Xe isotopes, ^{128}Xe and ^{130}Xe are primordial, ^{129}Xe was produced by the β-decay of the extinct nuclide ^{129}I ($t_{1/2}$=15.7 Ma), and ^{131,132,134,136}Xe are produced in characteristic relative proportions by spontaneous fission of both extinct ^{244}Pu ($t_{1/2}$=80.0 Ma) and extant ^{238}U ($t_{1/2}$=4.468 Ga). Consequently, Xe isotopic compositions of mantle-derived basalts provide information about the timing and extent of mantle degassing and the differentiation of the early Earth (i.e., up to ~500 Ma after accretion; Allègre et al., 1987; Kunz et al., 1998; Mukhopadhyay, 2012; Pepin and Porcelli, 2002; Staudacher and Allegre, 1982; Yokochi and Marty, 2004).

The majority of noble gas studies of mantle-derived rocks have, however, focused on He and Ne isotopic measurements, as measurements of mantle Ar and Xe are complicated by low abundances and pervasive syn- to post-eruptive atmospheric contamination. Existing He isotopic measurements in mantle-derived rocks indicate distinct degassing histories for the mantle sources of OIBs and MORBs. Basalts erupted at ocean islands exhibit a wide range of ^{4}He/^{3}He ratios, from ~14,000–170,000 (^{3}He/^{4}He of 50–4.1 R_A; Graham et al., 1992; Moreira et al., 1999; Stuart et al., 2003). Basalts erupted at mid-ocean ridges exhibit a more limited range of He isotopic compositions. MORB He isotopes are generally discussed with respect to a narrow "canonical" MORB ^{4}He/^{3}He range of 80,000–100,000 (^{3}He/^{4}He of 9–7 R_A). However, basalts from the ultra-slow spreading Southwest Indian Ridge (SWIR) from 7°E to 25°E exhibit ^{4}He/^{3}He ratios from 48,300–120,000 (14.9–6.0 R_A; Georgen et al., 2003; Kurz et al., 1998; Standish, 2006), spanning half the range observed in OIBs. ^{4}He/^{3}He values above and below the canonical MORB range are found in basalts erupted in close proximity. Additionally, Georgen et al. (2003) observe a smooth spatial gradient in helium isotopic composition in the western half of the study area. The remarkable variability and spatial gradient in helium isotopic compositions suggest that the SWIR between 7°E and 25°E affords a unique window into the nature and distribution of heterogeneities in the MORB source.

The extent of heterogeneity in MORB source Ar and Xe isotopic compositions is poorly constrained at present, as determinations of MORB source Ar and Xe isotopic compositions have been limited to a few very gas-rich samples (e.g., N. Atlantic popping rock 2ΠD43, Kunz et al., 1998; Moreira et al., 1998; Harding County well gases, Caffee et al., 1999; Holland and Ballentine, 2006; Phinney et al., 1978; Staudacher, 1987). However, a number of studies have demonstrated that the heavy noble gases (Ne, Ar and Xe) provide information on the origin of mantle heterogeneities that may not be evident in He or lithophile isotope systematics alone (e.g., Hanyu et al., 2001; Harrison et al., 1999; Holland and Ballentine, 2006; Honda and McDougall, 1998; Honda and Woodhead, 2005; Kunz et al., 1998, 2005; Moreira et al., 1998, 2011; Mukhopadhyay, 2012; Parai et al., 2009; Sarda et al., 2000; Tucker et al., 2012; Yokochi and Marty, 2004). For example, Holland and Ballentine (2006) used primordial heavy noble gas isotopes (e.g., ^{36}Ar, ^{130}Xe) measured in continental well gases to demonstrate that the MORB source heavy noble gas abundance pattern is similar to seawater, and suggested that unradiogenic ^{40}Ar/^{36}Ar and ^{129}Xe/^{130}Xe in OIBs reflect preferential recycling of atmospheric heavy noble gases into the OIB source relative to the MORB source. In contrast, Mukhopadhyay (2012) used Ne, Ar and Xe isotope systematics in Icelandic basalt glass to demonstrate that the Iceland plume and MORB source Ar and Xe cannot be related to each other solely through preferential recycling of atmospheric volatiles. Rather, the MORB and Iceland sources must have differentiated early in Earth history and have not been homogenized by ≥4.45 Ga of mantle convection (Mukhopadhyay, 2012). Thus, heavy noble gas systematics in mantle-derived samples can fundamentally improve our understanding of mantle evolution. In order to better constrain the extent and nature of heterogeneity in MORB source Ne, Ar and Xe isotopic compositions, we present new high-precision Ne, Ar and Xe isotopic compositions and abundances along with He and CO_2 abundances in a suite of basalt glasses from the SWIR between 7°E and 25°E.

2. Background and methods

2.1. Sample background

Fourteen submarine basalt glass samples erupted along the SWIR between 7°E and 25°E (Fig. 1) were selected for heavy noble gas analysis. The samples were previously characterized for major element, trace element and radiogenic lithophile isotopic compositions (Kurz et al., 1998; Mahoney et al., 1992; Standish, 2006, 2008) as well as helium concentrations and isotopic compositions (Georgen et al., 2003; Kurz et al., 1998; Standish, 2006). Samples from a single dredge located at the 7°E ridge segment, adjacent to Bouvet Island, illustrate the lengthscale of helium isotopic heterogeneity at the SWIR: one sample exhibits ^{4}He/^{3}He within the canonical MORB range (96,400; Kurz et al., 1998), while two other samples from the same dredge exhibit low ^{4}He/^{3}He ratios (48,300 and 51,000; Kurz et al., 1998). In the center of the study area between the Shaka Fracture Zone (FZ) and 16°E, ridge orientation is highly oblique to the spreading direction, resulting in a low effective spreading rate (Standish et al., 2008). This part of the ridge is known as the Oblique Supersegment and is characterized

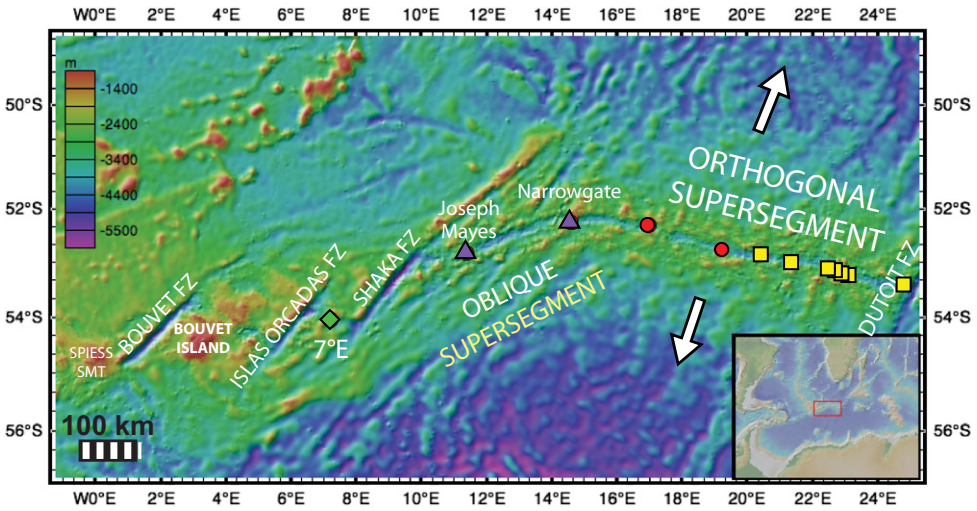

Fig. 1. Map of the Southwest Indian Ridge study area. The study area is bounded in the west by the Islas Orcadas Fracture Zone (FZ) and by the Dutoit FZ in the east. Bouvet Island is located ~200 km west of the study area. Some samples from 7°E exhibit low $^4He/^3He$ ratios (~48,300; Kurz et al., 1998). Other samples from 7°E exhibit $^4He/^3He$ ratios within the canonical MORB range (80,000–100,000). The Oblique Supersegment runs from 9°E to 16°E. Basalts erupted at the Joseph Mayes and Narrowgate Seamounts have very radiogenic $^4He/^3He$ (up to ~120,000; Supplementary Table S1). At the 16°E discontinuity, ridge orientation shifts such that spreading direction is nearly orthogonal to the ridge. The ~630 km long Orthogonal Supersegment exhibits $^4He/^3He$ ratios that vary smoothly from ~110,000 in the west to ~100,000 in the east (Georgen et al., 2003).

by amagmatic accretionary ridge segments punctuated by two discrete magmatic segments (Dick et al., 2003) that erupt basalts with the most radiogenic $^4He/^3He$ ratios measured in the area (up to ~120,000; Standish, 2006; Supplementary Table S1). Ridge orientation changes abruptly at the 16°E discontinuity, and the ridge is nearly orthogonal to the spreading direction between 16°E and the Dutoit FZ. A spatial gradient in helium isotopic composition is evident across the Orthogonal Supersegment, with $^4He/^3He$ decreasing smoothly from west to east over 630 km of ridge (Georgen et al., 2003).

2.2. Analytical methods

Basalt glass was chipped from pillow lavas. Chips exhibiting light surface alteration were leached in dilute nitric acid for 10–15 min and ultrasonically cleaned. Clean glass chips were washed in acetone and dried. Two to five grams of glass were loaded into a stainless steel piston crusher, baked at ~90–100 °C for 24 h, and then pumped for an additional 7–14 days until blanks were low and stable. To release magmatic gases trapped in vesicles, samples were step-crushed under ultra-high vacuum using a hydraulic ram. CO_2 contents were measured by manometers attached directly to the crusher volume. Active gases were removed by sequential exposure to hot and cold SAES getters. The noble gases were trapped on a cryogenic cold finger and sequentially released to the mass spectrometer volume. He, Ne, Ar and Xe abundances and Ne, Ar and Xe isotopic compositions were measured on a Nu Noblesse noble gas mass spectrometer operating in multicollection mode. Data were obtained over 2 years in four sets of measurements. For Ne, an automated liquid nitrogen trap was used to keep Ar and CO_2 blanks low, and corrections for isobaric interference from doubly-charged Ar and CO_2 were made. Ar^{++}/Ar^{+} for the four sets of SWIR analyses were 0.031 ± 0.003, 0.077 ± 0.003, 0.078 ± 0.003 and 0.061 ± 0.001; and CO_2^{++}/CO_2^{+} were 0.0045 ± 0.0005, 0.0055 ± 0.0003, 0.0079 ± 0.0006 and 0.0055 ± 0.0003. Procedural blanks were monitored during the step-crushing process. Blanks were stable and typically $<1\%$ of the measured sample ^{20}Ne signal, $<0.5\%$ of the measured sample ^{40}Ar signal and ~2% of the measured sample ^{130}Xe signal. All measured sample Ne, Ar and Xe isotope ratios reflect some degree of post-eruptive air contamination. Since blanks were low and statistically indistinguishable from air in isotopic composition, no blank corrections were made to the abundances or isotope ratios reported in Supplementary Table S1. Each sample step-crush was bracketed by multiple air standard runs, which were used to calibrate sensitivity and mass discrimination as a function of signal size. A total of 1280 heavy noble gas air standard runs were analyzed over the 2 year SWIR analytical campaign, with $\sim 10^{-11}$ to 10^{-9} cc STP ^{20}Ne, $\sim 10^{-9}$ to 10^{-8} cc STP ^{40}Ar and $\sim 10^{-15}$ to 10^{-13} cc STP ^{130}Xe. Uncertainties in Ne, Ar and Xe isotope ratios for each step-crush are based on the reproducibility of air standards of comparable signal size analyzed within the same time period.

3. Results

Fourteen samples were analyzed for He, Ne, Ar, Xe and CO_2 abundances, and Ne, Ar and Xe isotopic compositions. Multiple step-crush analyses were performed for each sample (3–23 steps per sample), giving a total of 169 SWIR analyses. The results are reported in Supplementary Table S1 and discussed below.

3.1. CO_2–Helium systematics

For each sample, individual crushing steps define a linear array in CO_2–^3He space, which we use to calculate a $CO_2/^3He$ ratio using a linear least squares fit (Supplementary Fig. S1). Following Marty and Tolstikhin (1998), this ratio is corrected for degassing following a Rayleigh fractionation law constrained by $^4He/^{40}Ar^*$ ratios (where $^{40}Ar^*$ denotes radiogenic mantle-derived ^{40}Ar):

$$\left(\frac{CO_2}{^3He}\right)_i = \left(\frac{CO_2}{^3He}\right)_{measured} \times \left(\frac{\left(^4He/^{40}Ar^*\right)_{measured}}{\left(^4He/^{40}Ar^*\right)_i}\right)^{\left[\left(1-(K_{He}/K_{CO_2})\right)/\left(1-(K_{He}/K_{Ar})\right)\right]} \quad (1)$$

where $(^4He/^{40}Ar^*)_i$ is the mantle source $^4He/^{40}Ar$ ratio of 2.5 and K denotes a solubility coefficient ($K_{Ar}=2.6\times10^{-12}$ mol/g·hPa, $K_{CO_2}=9.0\times10^{-12}$ mol/g·hPa, $K_{He}=2.5\times10^{-11}$ mol/g·hPa; Marty

Table 1
Mantle source $CO_2/^3He$ and He, Ne, Ar and Xe isotopic compositions. 1σ uncertainties reported for $^{40}Ar/^{36}Ar_{(E)}$ and $^{129}Xe/^{130}Xe_{(E)}$ are 68.3% confidence limits (Section 4.2).

Sample	Longitude (°E)	$^4He/^3He$	$CO_2/^3He$ ($\times 10^8$)	$^{21}Ne/^{22}Ne_{(E)}$	1σ	$^{40}Ar/^{36}Ar_{(E)}$	1σ	$^{129}Xe/^{130}Xe_{(E)}$	1σ
All107-6 57-9	7.260	48,300[a]	7.2	0.0414	0.0019	12,200	+1600 −1100	7.49[b]	−0.68
All107-6 57-25	7.260	51,000[a]	11	0.0424	0.0017	n.d.		n.d.	
All107-6 57-5	7.260	96,400[a]	29	0.0614	0.0006	23,700	+3400 −2400	6.89	+0.39 −0.14
KN162-9 33-49	11.387	120,000[c]	370	n.d.		n.d.		n.d.	
VAN7 89-02	14.598	119,000[d]	84	0.0624	0.0005	n.d.		n.d.	
AG22 1-1 and 1-4	16.980	108,000[d]	16	0.0680	0.0004	49,300	+6000 −4600	7.57	+0.18 −0.14
KN162-7 11-25	19.200	104,000[e]	9.8	0.0661	0.0004	43,400	+1800 −1800	7.80	+0.10 −0.10
KN162-7 14-7	20.398	104,000[e]	21	n.d.		n.d.		n.d.	
KN162-7 18-17	21.406	102,000[e]	8.3	0.0647	0.0007	23,600	+2600 −1700	n.d.	
KN162-7 23-107	22.547	98,900[e]	5.7	0.0678	0.0005	27,200	+2300 −1700	n.d.	
KN162-7 22-14	22.647	102,000[e]	11	0.0672	0.0005	20,500[f]		7.10	+0.04 −0.02
AG22 9-2	22.880	99,500[e]	4.8	0.0627	0.0013	n.d.		n.d.	
AG22 13-1	24.758	99,000[e]	10	0.0643	0.0011	29,200	+11900 −5900	7.19	+0.12 −0.09

[a] Kurz et al. (1998).
[b] The upper bound on the $^{129}Xe/^{130}Xe_{(E)}$ confidence interval for All107-6 57-9 is not well-determined (see Supplementary Fig. S3).
[c] Standish (2006).
[d] This study.
[e] Georgen et al. (2003).
[f] The $^{40}Ar/^{36}Ar_{(E)}$ confidence interval for KN162-7 22-14 is not well-determined (see Supplementary Fig. S2).

and Tolstikhin, 1998 and references therein). The magnitude of the degassing correction is uncertain for samples with near-atmospheric $^{40}Ar/^{36}Ar$ (such as KN162-9 33-49); however, we note that the measured $CO_2/^3He$ for KN162-9 33-49 itself is strikingly high (2.2×10^{10}), and correction for magmatic degassing only raises $CO_2/^3He$ (since $K_{CO_2} < K_{He}$; see Supplementary Fig. S1). It is possible that this sample's measured ratio has been affected by assimilation of seawater. However, even if KN162-9 33-49 is ignored, the $CO_2/^3He$ ratios in primary SWIR melts vary from 4.8×10^8 to 8.4×10^9 (Table 1) and thus reach values far in excess of the estimated average N-MORB value of ~1–2×10^9 (Marty and Tolstikhin, 1998).

3.2. Measured Ne, Ar, Xe compositions

We measure $^{20}Ne/^{22}Ne$ values up to 12.41 ± 0.02 (1σ), and $^{21}Ne/^{22}Ne$ ratios up to 0.0653 ± 0.0010 (1σ), among the highest isotopic excesses with respect to atmosphere ($^{20}Ne/^{22}Ne=9.80$, $^{21}Ne/^{22}Ne=0.0290$) measured in MORBs (Supplementary Table S1). Measured $^{40}Ar/^{36}Ar$ values vary up to $28{,}500\pm290$ (1σ). The highest measured isotopic ratio in $^{129}Xe/^{130}Xe$ is 7.71 ± 0.11 (1σ), which is comparable to the highest value measured in the popping rock 2ΠD43 ($^{129}Xe/^{130}Xe=7.73\pm0.23$; Moreira et al., 1998) and in Equatorial Atlantic MORBs ($^{129}Xe/^{130}Xe=7.81\pm0.06$; Tucker et al., 2012).

4. Source Ne, Ar and Xe isotopic compositions corrected for shallow-level air contamination

Variable syn- to post-eruptive air contamination affects all measurements of Ne, Ar and Xe in mantle-derived rocks (e.g., Ballentine and Barfod, 2000; Sarda et al., 1985), such that measured values represent mixing between the mantle source isotopic composition and the atmospheric composition. Corrections for shallow air contamination are required to accurately characterize mantle sources and interpret differences between mantle reservoirs. Variations in maximum measured Ar isotopic values have been discussed as indicative of source Ar isotopic heterogeneity (e.g., Sarda et al., 1999); however, maximum measured values may also reflect the degree of atmospheric contamination, which varies randomly or as a function of eruption depth (e.g., Burnard, 1999). Therefore, variations in maximum measured values may not accurately reflect heavy noble gas isotope systematics in mantle sources.

Well-defined arrays in $^{20}Ne/^{22}Ne$–$^{21}Ne/^{22}Ne$, $^{40}Ar/^{36}Ar$–$^{20}Ne/^{22}Ne$ and $^{129}Xe/^{130}Xe$–$^{40}Ar/^{36}Ar$ spaces allow us to determine mantle source isotopic compositions by least-squares fitting and extrapolation to a mantle $^{20}Ne/^{22}Ne$ value. We use a $^{20}Ne/^{22}Ne$ value of 12.5 for the MORB source (Holland and Ballentine, 2006; Ballentine and Holland, 2008; Raquin et al., 2008), though correcting to the solar wind composition ($^{20}Ne/^{22}Ne$ of 13.8) would not alter our conclusions. Correction for air contamination is a total least-squares linear extrapolation for mantle $^{21}Ne/^{22}Ne$ (Fig. 2), and a total least-squares hyperbolic extrapolation for mantle $^{40}Ar/^{36}Ar$ (Fig. 3). The extrapolated mantle $^{40}Ar/^{36}Ar$ can then be used in a total least-squares hyperbolic extrapolation for mantle $^{129}Xe/^{130}Xe$ (Fig. 4). Extrapolations are only performed for samples with well-defined mixing arrays. We note that AG22 1-1 and 1-4 overlap in every isotope space; these are likely to sample a single flow and are therefore considered together for extrapolation. Below we discuss SWIR mantle source Ne, Ar and Xe isotopic compositions corrected for the effects of shallow air contamination.

4.1. Mantle source neon isotopic compositions

For each SWIR sample, step-crushes define a linear array trending toward the atmospheric composition that reflects variable degrees of atmospheric contamination in $^{20}Ne/^{22}Ne$–$^{21}Ne/^{22}Ne$ space. To correct for air contamination, the data are translated to fix the atmospheric composition at the origin and a total least-squares fit of the form $y=mx$ (to force the fit through air) is determined by minimizing χ^2 given errors in both variables (after York, 1969). Uncertainties in the slopes are determined by Monte Carlo error analysis: for each sample, data

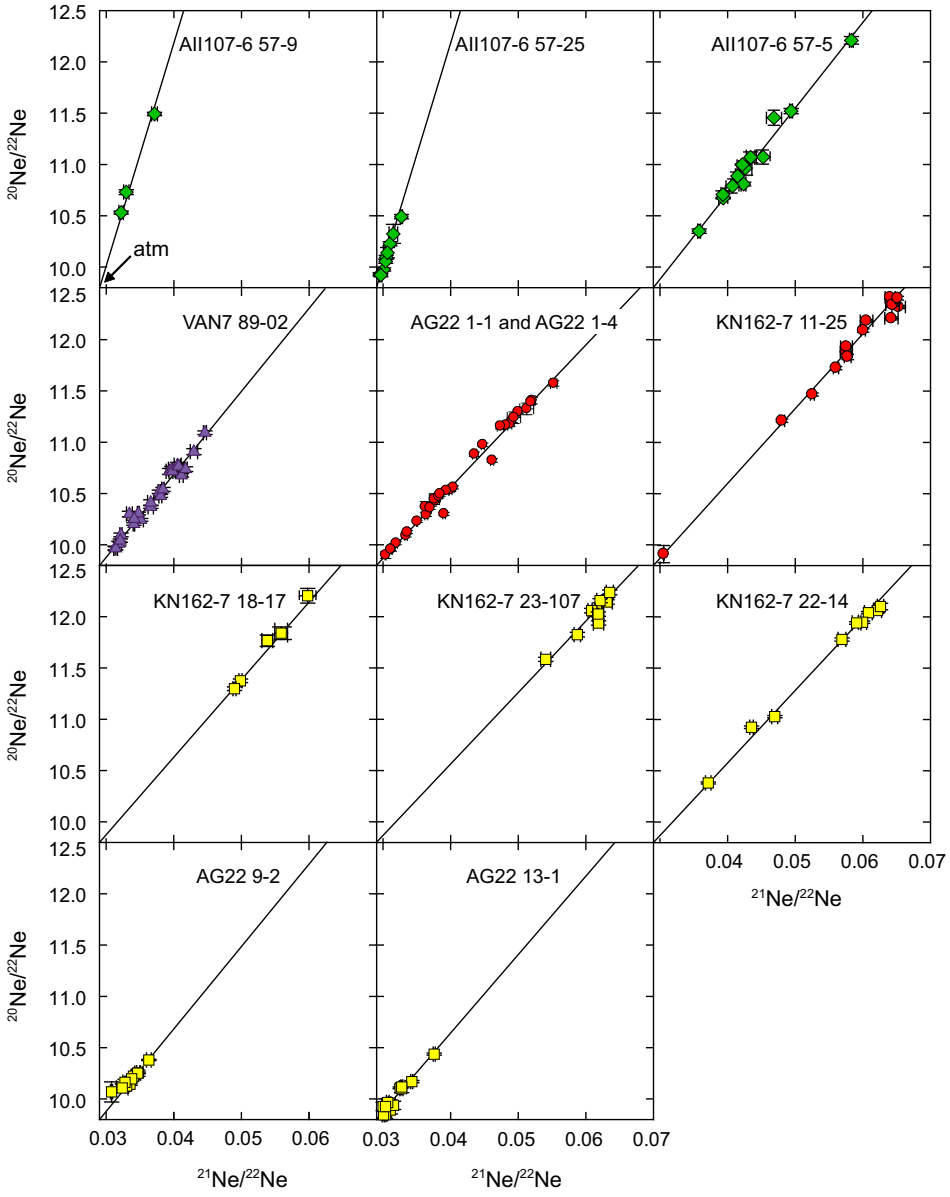

Fig. 2. Ne three-isotope space. For each sample, step-crushing generates a linear array reflecting variable degrees of atmospheric contamination. Each sample is corrected for air contamination by total least squares regression (Section 4.1) and extrapolation to determine the source $^{21}Ne/^{22}Ne_{(E)}$ at a mantle $^{20}Ne/^{22}Ne$ of 12.5.

are randomly resampled from within the bivariate normal distributions associated with each data point, and the least-squares fit is recomputed using the new values. Well-defined slopes allow us to determine extrapolated mantle source $^{21}Ne/^{22}Ne_{(E)}$ at $^{20}Ne/^{22}Ne = 12.5$ with high precision (Fig. 2; extrapolations are not performed for samples KN162-7 14-7 and KN162-9 33-49, since all crushing steps are close to atmospheric in composition). The extrapolated mantle source Ne compositions range from $^{21}Ne/^{22}Ne_{(E)} = 0.0414 \pm 0.0020$ (1σ) at 7°E to $^{21}Ne/^{22}Ne_{(E)} = 0.0680 \pm 0.0004$ (1σ) at the western Orthogonal Supersegment (Table 1).

4.2. Mantle source argon isotopic compositions

Air contamination generates hyperbolic trends in $^{40}Ar/^{36}Ar$–$^{20}Ne/^{22}Ne$ space. A best-fit hyperbola reflecting two-component mixing between air and mantle is determined using a total least-squares hyperbolic fit. The curvature of a two-component mixing hyperbolic array is parameterized as $k = (^{36}Ar/^{22}Ne)_{mantle}/(^{36}Ar/^{22}Ne)_{atm}$. We use a grid search to find the combination of k and mantle $^{40}Ar/^{36}Ar$ (corresponding to a mantle $^{20}Ne/^{22}Ne$ of 12.5) that minimizes the χ^2 cost function:

$$\chi^2 = \sum_{i=1}^{N} \left[\left(\frac{x_i - m_i}{\sigma_{xi}} \right)^2 + \left(\frac{y_i - n_i}{\sigma_{yi}} \right)^2 \right] \quad (2)$$

where $(x_i \pm \sigma_{xi}, y_i \pm \sigma_{yi})$ are the N observed data points for a given sample and (m_i, n_i) are the σ-normalized closest points to the data along a candidate hyperbola (i.e., the points that minimize χ^2 for the candidate hyperbola). Since there are two free parameters in the hyperbolic fit (k and mantle $^{40}Ar/^{36}Ar$), the 68.3% confidence interval on the mantle $^{40}Ar/^{36}Ar$ (Table 1) is where $\chi^2 \leq \chi^2_{min} + 2.30$ (e.g., Press et al., 1992; see Supplementary Fig. S2).

For some samples, scatter in the mixing array is much larger than the analytical uncertainties and likely reflects the influence of a second elementally-fractionated air component. Three-component mixing between mantle and two atmospheric components with distinct $^{36}Ar/^{22}Ne$ ratios would generate an array of measured values constrained to lie within a crescent or lens-

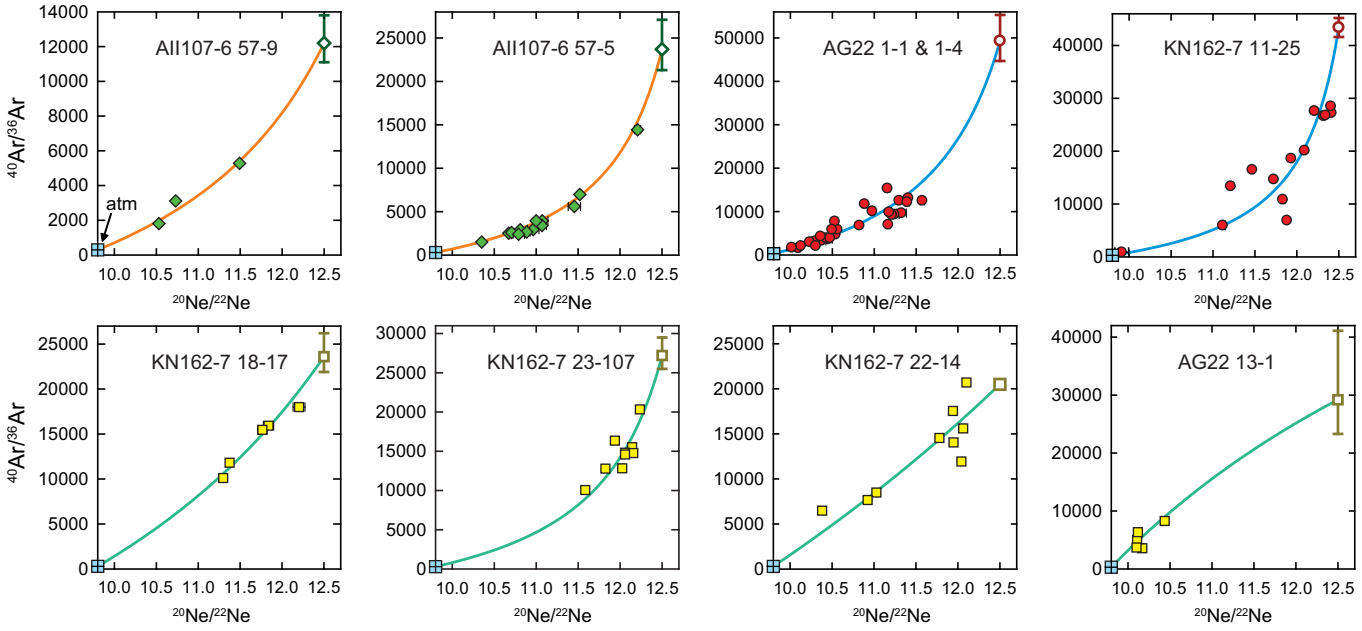

Fig. 3. Correction for shallow-level air contamination to determine mantle source $^{40}Ar/^{36}Ar$. For each sample, step-crushing generates an array reflecting variable degrees of atmospheric contamination. For samples with well-defined hyperbolic mixing arrays in $^{40}Ar/^{36}Ar$–$^{20}Ne/^{22}Ne$ space, best fit hyperbolae yield extrapolated mantle $^{40}Ar/^{36}Ar_{(E)}$ at $^{20}Ne/^{22}Ne=12.5$. AG22 1–1 and AG22 1–4 were brought up in the same dredge and therefore could sample the same flow. Since major element compositions (Standish, 2006) and isotopic compositions in all heavy noble gas spaces were nearly identical, we considered AG22 1–1 and 1–4 together to better constrain the hyperbolic fits.

shaped region. Random sampling of data from within such a region would not necessarily provide a good constraint on the mantle endmember $^{40}Ar/^{36}Ar$. Therefore, we restrict our extrapolations to samples with relatively well-defined hyperbolic mixing arrays (eight extrapolations; Fig. 3). Such hyperbolic arrays are likely to reflect either a single atmospheric contaminant or two elementally-fractionated atmospheric contaminants present in nearly fixed proportions. Mantle $^{40}Ar/^{36}Ar_{(E)}$ values range from $12{,}200^{+1600}_{-1100}$ at 7°E to $49{,}300^{+6000}_{-4600}$ in the western Orthogonal Supersegment (Table 1).

4.3. Mantle source xenon isotopic compositions

Air contamination generates hyperbolic trends in $^{129}Xe/^{130}Xe$–$^{20}Ne/^{22}Ne$ and $^{129}Xe/^{130}Xe$–$^{40}Ar/^{36}Ar$ space. Best-fit hyperbolae reflecting two-component mixing between atmosphere and mantle are determined as described in Section 4.2. The fits yield extrapolated mantle source $^{129}Xe/^{130}Xe_{(E)}$ values at the mantle $^{40}Ar/^{36}Ar_{(E)}$ values determined above (six extrapolations; Fig. 4). Since the best fits have pronounced concave-down curvatures, the extrapolated $^{129}Xe/^{130}Xe_{(E)}$ is only weakly sensitive to uncertainty in the mantle $^{40}Ar/^{36}Ar_{(E)}$; therefore, the 68.3% confidence limits on $^{129}Xe/^{130}Xe_{(E)}$ are given assuming the best $^{40}Ar/^{36}Ar_{(E)}$. Mantle $^{129}Xe/^{130}Xe_{(E)}$ values range from $6.89^{+0.39}_{-0.19}$ to 7.80 ± 0.10 (Table 1).

5. Discussion

The SWIR between 7°E and 25°E is comprised of four compositionally distinct regions: the 7°E ridge segment, the Oblique Supersegment, the western Orthogonal Supersegment and the eastern Orthogonal Supersegment. Below we discuss the noble gas isotopic systematics observed in the study area and investigate the nature of MORB source noble gas heterogeneity. We then evaluate SWIR Xe isotope systematics and discuss the implications for early mantle differentiation. SWIR Xe fission isotopes and relationships between noble gases and major and trace element ratios will be discussed elsewhere.

5.1. Variations in MORB source composition along the SWIR from 7°E to 25°E

We observe remarkable and systematic variability in heavy noble gas isotopic composition across the ~1100 km-wide study area (Figs. 5–7). Fig. 5 illustrates systematic variations in mantle source $CO_2/^3He$ and Ne, Ar and Xe isotopic compositions as a function of longitude. Extremely high $CO_2/^3He$ ratios are observed at the Oblique Supersegment (Fig. 5a; 3.7×10^{10}), far in excess of the mean values estimated for N-MORB and E-MORB (~1 and $\sim 4 \times 10^9$, respectively; Marty and Tolstikhin, 1998). Across the Orthogonal Supersegment, we observe considerable variation in source Ne, Ar and Xe isotopic compositions over a short distance (~600 km). A broad spatial gradient is present in $^{21}Ne/^{22}Ne_{(E)}$, $^{40}Ar/^{36}Ar_{(E)}$ and $^{129}Xe/^{130}Xe_{(E)}$ (Fig. 5), though sample coverage across the Orthogonal Supersegment is not as dense as for $^4He/^3He$ (Georgen et al., 2003).

Fig. 6 illustrates He–Ne, He–Ar and Ne–Ar source systematics in SWIR samples, with N. Atlantic popping rock 2ΠD43 (Moreira et al., 1998), Equatorial Atlantic depleted MORB (Tucker et al., 2012), Bravo Dome continental well gas (Holland and Ballentine, 2006) and Icelandic DICE (Trieloff et al., 2000; Mukhopadhyay, 2012) sources included for reference. We find a broad positive correlation between SWIR source He, Ne and Ar isotopic compositions, and SWIR source co-variations are consistent with the differences between the relatively undegassed DICE source and the N. Atlantic MORB source. The low $^4He/^3He$ samples from 7°E are similar to DICE in all panels. We note that Eastern Orthogonal Supersegment source values are more radiogenic in He and more nucleogenic in Ne than the N. Atlantic source, but are low or comparable in $^{40}Ar/^{36}Ar_{(E)}$.

Fig. 7 shows He–Xe, Ne–Xe and Ar–Xe source systematics in the same samples. Relatively low $^4He/^3He$, $^{21}Ne/^{22}Ne_{(E)}$ and $^{40}Ar/^{36}Ar_{(E)}$ in the eastern Orthogonal Supersegment are associated with $^{129}Xe/^{130}Xe_{(E)}$ that are low (~7.1) compared to 2ΠD43 and

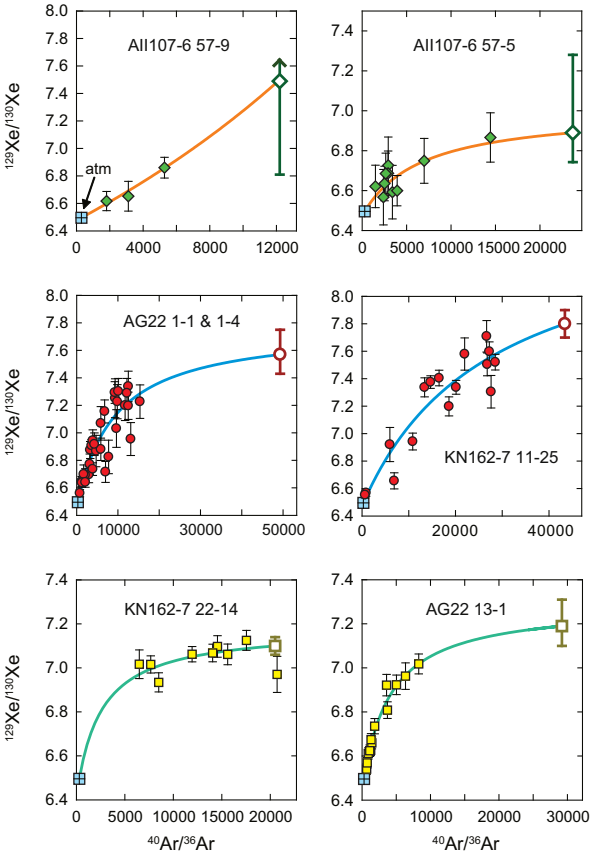

Fig. 4. Correction for shallow-level air contamination to determine mantle source $^{129}Xe/^{130}Xe$. For each sample, step-crushing generates an array reflecting variable degrees of atmospheric contamination. For samples with well-defined hyperbolic mixing arrays in $^{129}Xe/^{130}Xe$–$^{40}Ar/^{36}Ar$ space, best fit hyperbolae yield extrapolated mantle $^{129}Xe/^{130}Xe_{(E)}$ at the $^{40}Ar/^{36}Ar_{(E)}$ determined in Fig. 3. Mixing arrays in $^{20}Ne/^{22}Ne$–$^{129}Xe/^{130}Xe$ space exhibit more scatter, but are in good agreement with $^{129}Xe/^{130}Xe$–$^{40}Ar/^{36}Ar$ results. Three data points with subatmospheric $^{129}Xe/^{130}Xe$ in All107-6 57-5 were excluded from the fit. The upper limit of the 68.3% confidence interval for All107-6 57-9 is poorly constrained and is thus depicted by an upward arrow.

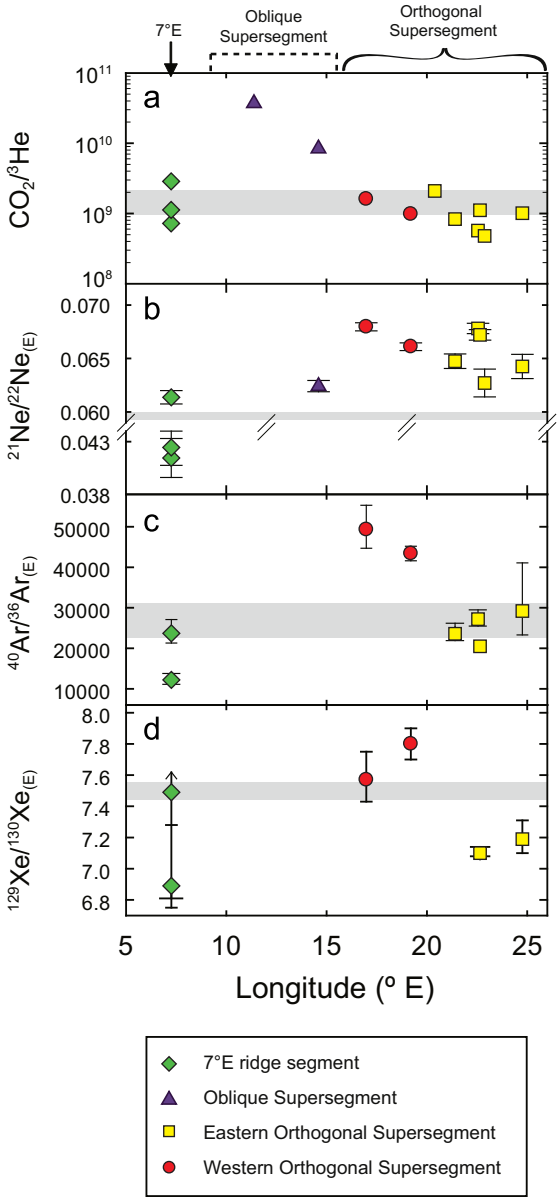

Fig. 5. Mantle source $CO_2/^3He$, Ne, Ar and Xe isotopic variations with longitude along the SWIR from 7°E to 25°E. Shaded band indicates the average N-MORB estimate (panel (a); Marty and Tolstikhin, 1998) and N. Atlantic popping rock 2ΠD43 source composition (panels (b–d); Moreira et al., 1998; Raquin et al., 2008). (a) $CO_2/^3He$ corrected for degassing following a Rayleigh fractionation law (see Section 3.1) is plotted on a logarithmic scale against longitude. $CO_2/^3He$ in basalts from 7°E and the Orthogonal Supersegment scatter around typical N-MORB values of $\sim 1–2 \times 10^9$. A large anomaly in $CO_2/^3He$ is observed at the Oblique Supersegment. (b) Mantle source $^{21}Ne/^{22}Ne_{(E)}$ vs. longitude. Along the Orthogonal Supersegment, $^{21}Ne/^{22}Ne_{(E)}$ broadly decreases from west to east. (c) Mantle source $^{40}Ar/^{36}Ar_{(E)}$ vs. longitude. A broad gradient in $^{40}Ar/^{36}Ar_{(E)}$ is evident across the Orthogonal Supersegment. (d) Mantle source $^{129}Xe/^{130}Xe_{(E)}$ vs. longitude. Fewer samples are plotted here since mixing hyperbolae for some samples were poorly constrained. Two distinct groupings are also evident in $^{129}Xe/^{130}Xe_{(E)}$ along the Orthogonal Supersegment: a relatively radiogenic group in the west and a less-radiogenic group in the eastern half of the supersegment.

approaching $^{129}Xe/^{130}Xe_{(E)}$ for DICE. On the other hand, western Orthogonal Supersegment source $^{129}Xe/^{130}Xe_{(E)}$ ratios range from ~7.6–7.8, slightly higher than the value of ~7.6 in 2ΠD43 (Moreira et al., 1998) and within the range of 7.9 ± 0.14 for the mantle source of continental well gas (Holland and Ballentine, 2006). Significantly, the magnitude of variation in Orthogonal Supersegment $^{40}Ar/^{36}Ar_{(E)}$ and $^{129}Xe/^{130}Xe_{(E)}$ is much larger than the relative variation in $^4He/^3He$ and $^{21}Ne/^{22}Ne_{(E)}$ (Figs. 6 and 7). Low source $^{40}Ar/^{36}Ar_{(E)}$ and $^{129}Xe/^{130}Xe_{(E)}$ at the eastern Orthogonal Supersegment may be related to recycling of atmospheric Ar and Xe (see Sections 5.3.3 and 5.3.4). We note that the sample from 7°E with the $^4He/^3He$ ratio of 96,400 (Table 1) groups with the eastern Orthogonal Supersegment in all isotope spaces (Figs. 6 and 7).

5.2. *A heterogeneous MORB source mantle in heavy noble gas isotopes*

Lithophile isotopic variations in mantle sources are often interpreted with respect to a set of theoretical endmember components, such as the depleted MORB mantle (DMM), HIMU, EMI and EMII (enriched mantles I and II). These theoretical endmember compositions are based on compiled lithophile isotopic measurements of mantle-derived rocks (e.g., Hart et al., 1992; Zindler and Hart, 1986; Zindler et al., 1982). Given the scarcity of precise heavy noble gas isotopic data exhibiting clear excesses from air, the magnitude of variation in mantle source heavy noble gas isotopic composition and the specific signatures associated with established mantle endmember components are poorly constrained. However, the variability in source Ne, Ar and Xe isotopic compositions we observe along the SWIR Orthogonal Supersegment

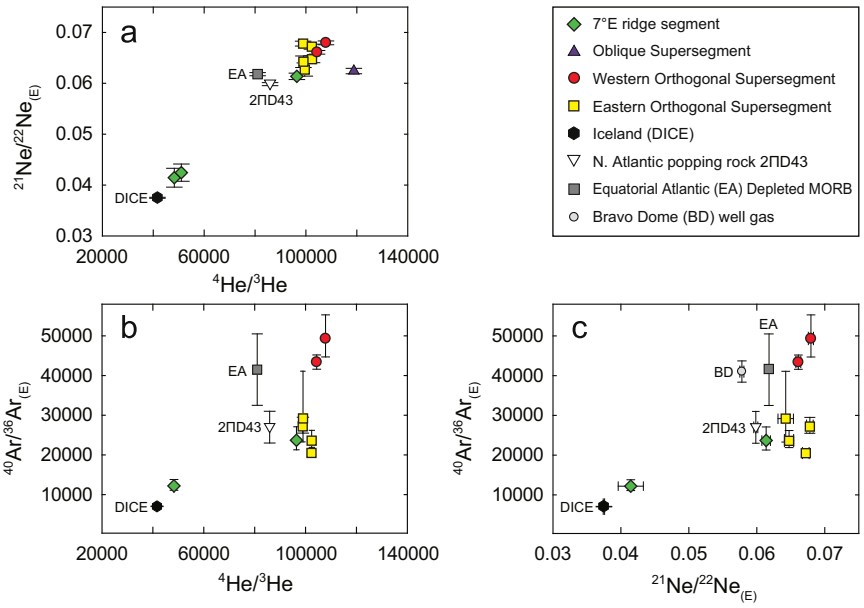

Fig. 6. (a) He–Ne, (b) He–Ar and (c) Ne–Ar systematics in SWIR mantle sources. SWIR mantle source He, Ne and Ar isotopic compositions behave coherently, such that low $^{4}He/^{3}He$ ratios are associated with low $^{21}Ne/^{22}Ne_{(E)}$ and low $^{40}Ar/^{36}Ar_{(E)}$, and high $^{4}He/^{3}He$ ratios are associated with high $^{21}Ne/^{22}Ne_{(E)}$ and high $^{40}Ar/^{36}Ar_{(E)}$. N. Atlantic popping rock 2ΠD43 (Moreira et al., 1998; Raquin et al., 2008), Equatorial Atlantic depleted MORB (Tucker et al., 2012), Bravo Dome continental well gas (Holland and Ballentine, 2006) and the Icelandic glass DICE (Mukhopadhyay, 2012; Trieloff et al., 2000) sources are included for comparison. He–Ne–Ar systematics indicate the influence of a reservoir that is relatively undegassed compared to the N. Atlantic popping rock source and similar to the Iceland source, as well as at least two reservoirs that are degassed relative to the popping rock source. Eastern Orthogonal Supersegment source values are more radiogenic in He and more nucleogenic in Ne than the popping rock source, but are low or comparable in $^{40}Ar/^{36}Ar_{(E)}$.

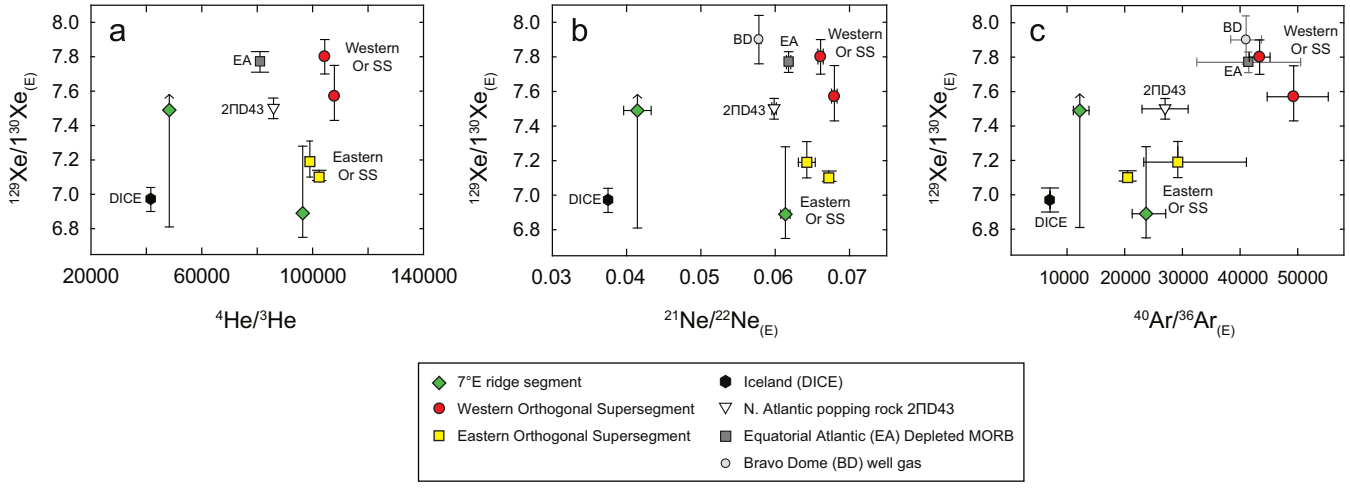

Fig. 7. (a) He–Xe, (b) Ne–Xe and (c) Ar–Xe systematics in SWIR mantle sources. N. Atlantic popping rock 2ΠD43 (Moreira et al., 1998; Raquin et al., 2008), Equatorial Atlantic depleted MORB (Tucker et al., 2012), Bravo Dome continental well gas source (Holland and Ballentine, 2006) and the Icelandic glass DICE (Mukhopadhyay, 2012; Trieloff et al., 2000) are included for comparison. The western and eastern Orthogonal Supersegments are clearly distinct in $^{129}Xe/^{130}Xe_{(E)}$, and large variations in Orthogonal Supersegment $^{129}Xe/^{130}Xe_{(E)}$ are associated with limited variations in He and Ne isotopic composition. Low $^{129}Xe/^{130}Xe_{(E)}$ in the eastern Orthogonal Supersegment group is paired with intermediate $^{40}Ar/^{36}Ar_{(E)}$ (panel (c)). The low $^{4}He/^{3}He$ sample from 7°E is characterized by intermediate $^{129}Xe/^{130}Xe_{(E)}$, although the extrapolation is based on only three data points (Fig. 4) and the upper limit uncertainty is poorly constrained. We note that the AII107-6 57-5 sample from 7°E with a $^{4}He/^{3}He$ ratio of 96,400 plots with the eastern Orthogonal Supersegment samples in all noble gas isotope spaces (also see Fig. 6).

(Figs. 5–7) indicates that the MORB source is heterogeneous in heavy noble gas isotopic composition. Significant variation in Orthogonal Supersegment MORB source Ne, Ar and Xe exist independent of any known hotspot influence: $^{21}Ne/^{22}Ne_{(E)}$ varies from 0.0627 ± 0.0013 to 0.0680 ± 0.0004, $^{40}Ar/^{36}Ar_{(E)}$ from 20,500 to $49{,}300^{+6000}_{-4600}$ and $^{129}Xe/^{130}Xe_{(E)}$ from $7.10^{+0.04}_{-0.02}$ to 7.80 ± 0.10 (Figs. 5–7). We note that our argument for particularly large variation in MORB source $^{129}Xe/^{130}Xe$ is independent of the hyperbolic extrapolations: step-crushing data from KN162-7 22-14 in the eastern Orthogonal Supersegment indicate that $^{129}Xe/^{130}Xe$ values asymptote with respect to $^{40}Ar/^{36}Ar$ at $^{129}Xe/^{130}Xe$ of ~7.1, significantly lower than measured values of up to 7.71 ± 0.11 in the western Orthogonal Supersegment (Fig. 4). Therefore, the large variation in Orthogonal Supersegment source $^{129}Xe/^{130}Xe_{(E)}$ is robust.

We observe ~20%, 70% and 80% of the total mantle variation in $^{21}Ne/^{22}Ne_{(E)}$, $^{40}Ar/^{36}Ar_{(E)}$ and $^{129}Xe/^{130}Xe_{(E)}$ ratios, respectively, along the SWIR Orthogonal Supersegment (Figs. 5–7). In light of this source heterogeneity, interpreting any single MORB composition as representative of the average MORB source is problematic. However, geochemical reservoir models have used the composition of the gas-rich N. Atlantic popping rock 2ΠD43 (e.g., Moreira et al., 1998; Staudacher et al., 1989) as representative of the

average MORB source (e.g., Davies, 2010; Gonnermann and Mukhopadhyay, 2009; Porcelli and Wasserburg, 1995; Tolstikhin and Marty, 1998) in order to constrain mass exchange between mantle reservoirs. Given the observed large variation in isotopic composition and the small number of mantle source Ar and Xe isotopic constraints, the average Ar and Xe isotopic compositions of the MORB source are probably not yet well-defined.

5.3. The nature of the heterogeneities observed at SWIR 7–25°E

5.3.1. The 7°E ridge segment

Low $^{4}He/^{3}He$, $^{21}Ne/^{22}Ne_{(E)}$ and $^{40}Ar/^{36}Ar_{(E)}$ and intermediate $^{129}Xe/^{130}Xe_{(E)}$ at 7°E indicate the influence of a relatively undegassed reservoir in the westernmost SWIR, which may be related to the Bouvet plume (Fig. 1). The data are consistent with previous studies of plume-related heavy noble gases (Figs. 6 and 7), indicating that less-nucleogenic $^{21}Ne/^{22}Ne_{(E)}$, less-radiogenic $^{40}Ar/^{36}Ar_{(E)}$ and less-radiogenic $^{129}Xe/^{130}Xe_{(E)}$ are characteristic of plume sources and do not result from syn- to post-eruptive air contamination. The close spatial association between the relatively undegassed and degassed source signatures indicates either that the SWIR source at 7°E is heterogeneous on very fine lengthscales, or that melts from spatially disparate mantle sources are channeled towards common volcanic centers and erupted without being completely homogenized.

5.3.2. The Oblique Supersegment

High $^{4}He/^{3}He$ ratios at the Oblique Supersegment reflect a source that is more degassed of primordial ^{3}He than the canonical MORB source. Such signatures are commonly attributed to the presence of recycled material in the mantle source (e.g., Graham et al., 1992; Hanyu et al., 1999; Hilton et al., 2000; Kurz et al., 1982; Moreira et al., 1999; Parai et al., 2009). The sample VAN7 89-02 exhibits $^{4}He/^{3}He$ that is amongst the most radiogenic in the study area (119,000; Supplementary Table S1); however, $^{21}Ne/^{22}Ne_{(E)}$ is only slightly nucleogenic compared to N. Atlantic popping rock (e.g., Figs. 5b and 6a). Both Oblique Supersegment samples were erupted at shallow depth (1400–2400 m), and hyperbolic arrays for Oblique Supersegment samples in $^{40}Ar/^{36}Ar$–$^{20}Ne/^{22}Ne$ and $^{129}Xe/^{130}Xe$–$^{40}Ar/^{36}Ar$ spaces are too poor to determine $^{40}Ar/^{36}Ar_{(E)}$ and $^{129}Xe/^{130}Xe_{(E)}$. Importantly, this sample has a $CO_2/^{3}He$ ratio of 8.4×10^{9}, which is a factor of >3 larger than the averages for both MORBs and OIBs (Marty and Tolstikhin, 1998). While carbonate may be recycled back to the mantle in significant quantities (e.g., Dasgupta et al., 2004; Huang et al., 2011), ^{3}He is not recycled back to the mantle. Consequently, the high $CO_2/^{3}He$ ratio would be consistent with CO_2 enrichment of the mantle source associated with carbonate-bearing recycled material. Elevated $CO_2/^{3}He$ may also reflect shallow assimilation of altered oceanic crust (e.g., Marty et al., 2001). However, there is no obvious evidence of shallow crustal assimilation in Oblique Supersegment trace element and lithophile isotopic compositions (Standish, 2006), and so the signature of shallow crustal assimilation would have to be limited to $CO_2/^{3}He$.

Based on major element, trace element and lithophile isotopic data, Le Roex et al. (1992) argued that the alkali-enriched signature at the Oblique Supersegment reflected melting of a mantle source veined with frozen low-degree melts of Bouvet plume material. Such a process would generate strongly enriched major and trace element compositions at the Oblique Supersegment while preserving Bouvet isotopic compositions (Le Roex et al., 1992). However, radiogenic $^{4}He/^{3}He$ and nucleogenic $^{21}Ne/^{22}Ne_{(E)}$ are unlikely to be generated by preferential tapping of frozen low-degree melts of plume material at the Oblique Supersegment. Furthermore, CO_2 and He are both highly incompatible during partial melting and low-degree melts would not be sufficiently enriched in $CO_2/^{3}He$ to account for the 10-fold enhancement in the ratios at the Oblique Supersegment (Fig. 5a). Therefore, we suggest that at the Oblique Supersegment, a relatively degassed reservoir incorporating recycled material mixes with the ambient depleted mantle source.

5.3.3. The Orthogonal Supersegment

The spatial gradient in $^{4}He/^{3}He$ observed along the Orthogonal Supersegment (Georgen et al., 2003) may reflect sampling of a peridotite mantle veined with recycled oceanic crust (pyroxenite), with a gradient either in pyroxenite distribution or in mantle temperature along the SWIR (e.g., Georgen et al., 2003; Graham et al., 2001). More radiogenic $^{4}He/^{3}He$ signatures in the west could reflect a greater proportion of recycled pyroxenite in the source, or preferential melting of pyroxenite at low temperatures. Since recycled oceanic crust is heavily degassed, pyroxenite veins should either have negligible mantle-derived ^{129}Xe and ^{130}Xe or should carry atmospheric $^{129}Xe/^{130}Xe$ ratios. Hence, we would expect either minimal variability of $^{129}Xe/^{130}Xe$ across the Orthogonal Supersegment or lower $^{129}Xe/^{130}Xe$ ratios in the west due to the preferential sampling of recycled pyroxenite veins. However, $^{129}Xe/^{130}Xe_{(E)}$ at the western Orthogonal Supersegment are similar to the Equatiorial Atlantic depleted MORB and Bravo Dome continental well gas sources, and low $^{129}Xe/^{130}Xe_{(E)}$ are found in the eastern Orthogonal Supersegment (Fig. 7). Therefore, we suggest that differential sampling of pyroxenite veins embedded in a peridotite matrix does not explain the full suite of noble gas observations from the Orthogonal Supersegment.

A possible explanation for the differences in heavy noble gas composition along the Orthogonal Supersegment is that the eastern region samples a southern Indian Ocean mantle that is inherently characterized by low $^{40}Ar/^{36}Ar_{(E)}$ and $^{129}Xe/^{130}Xe_{(E)}$ (e.g., Sarda et al., 2000) compared to N. Atlantic mantle source. Thus, variation across the Orthogonal Supersegment could reflect sampling of distinct mantle domains in the east and west. In this regard, Mahoney et al. (1992) suggested that the SWIR Orthogonal Supersegment contained a boundary between the Atlantic MORB mantle and the Indian MORB mantle domain characterized by a Dupal Pb isotopic signature (elevated $^{207}Pb/^{204}Pb$ and $^{208}Pb/^{204}Pb$ at a given $^{206}Pb/^{204}Pb$, compared to the Northern Hemispheric Reference Line; Dupre and Allegre, 1983; Hart, 1984). Compared to the western Orthogonal Supersegment, the eastern Orthogonal Supersegment is characterized by a stronger Dupal Pb signature. The Dupal signature reflects ancient (>3 Ga) enrichment of Th/U and is often attributed to the incorporation of subcontinental lithospheric mantle (SCLM) throughout the Indian MORB source in association with the breakup of Gondwanaland (Hart, 1984; Hawkesworth et al., 1986; Mahoney et al., 1989, 1992; Storey et al., 1989). Samples from the S. Atlantic from 42°S to 50°S also exhibit the Dupal Pb signature (Douglass et al., 1999) and Sarda et al. (2000) argued that Dupal is associated with low source $^{40}Ar/^{36}Ar_{(E)}$ based on noble gas analyses of the same samples (corrected for shallow-level air contamination assuming linear mixing in $^{40}Ar/^{36}Ar$–$^{20}Ne/^{22}Ne$ space; Sarda et al., 2000). S. Atlantic $^{129}Xe/^{130}Xe$ maximum measured values are also low compared to N. Atlantic popping rock; however, source $^{129}Xe/^{130}Xe_{(E)}$ could not be determined due to large analytical errors and small excesses compared to atmosphere (Sarda et al., 2000). If the eastern Orthogonal Supersegment samples a Dupal mantle domain, then the observed low $^{40}Ar/^{36}Ar_{(E)}$ and low $^{129}Xe/^{130}Xe_{(E)}$ associated with slightly radiogenic He and nucleogenic Ne (compared to the N. Atlantic popping rock source) is characteristic of Dupal mantle, consistent with Sarda et al. (2000).

5.3.4. Constraints on the origin of the Dupal mantle domain

The Dupal Pb signature is commonly attributed to the incorporation of SCLM (> 3 Ga) into the southern Indian mantle source (e.g., Hart, 1984; Hawkesworth et al., 1986; Mahoney et al., 1989, 1992; Storey et al., 1989). Low $^{40}Ar/^{36}Ar$ ratios in the Dupal mantle domain could reflect evolution of SCLM with low $K/^{36}Ar$, which would effectively freeze the MORB source mantle $^{40}Ar/^{36}Ar$ ratio at the time of SCLM formation (Sarda et al., 2000). However, unmodified SCLM should be characterized by $^{129}Xe/^{130}Xe$ identical to the rest of the MORB source mantle since $^{129}Xe/^{130}Xe$ ratios stopped evolving ~100 Ma after the start of the Solar System, unless the SCLM is ancient (> 4.45 Ga). If SCLM is younger than 4.45 Ga, unradiogenic Ar and Xe in the Dupal mantle relative to N. Atlantic or Pacific mantle could reflect incorporation of noble gases from a distinct, relatively undegassed reservoir into SCLM. However, we see no geochemical evidence in He, Ne or any of the lithophile isotopes (Standish, 2006) for the presence a relatively undegassed mantle plume component. Therefore, we do not discuss this option further.

Alternatively, the low $^{40}Ar/^{36}Ar_{(E)}$ and $^{129}Xe/^{130}Xe_{(E)}$ in the Dupal mantle could reflect metasomatism of the SCLM by subduction zone fluids carrying atmospheric Ar and Xe without significant contributions of He and Ne. This conclusion would be consistent with recent studies indicating that atmospheric Ar and Xe are recycled into the mantle (Holland and Ballentine, 2006; Kendrick et al., 2011; Sumino et al., 2010). Furthermore, some previous studies (Matsumoto et al., 2001; Yamamoto et al., 2004) have argued for the introduction of atmospheric heavy noble gases into SCLM based on noble gas measurements in alpine peridotites and lithospheric mantle xenoliths. Gautheron et al. (2005) also observed low $^{40}Ar/^{36}Ar$ ratios in SCLM xenoliths, but favored shallow-level atmospheric contamination to explain the observed Ar isotopic systematics. If the Dupal Pb signature within our study area is due to delaminated SCLM in the mantle source, then low $^{129}Xe/^{130}Xe_{(E)}$ ratios in the eastern Orthogonal Supersegment source require either an age of formation > 4.45 Ga or more recent metasomatism of the SCLM by fluids carrying atmospheric Ar and Xe.

5.4. SWIR Xe evidence for upper mantle heterogeneity, early differentiation and preservation of ancient mantle reservoirs

Xe isotopic compositions of mantle-derived rocks provide information about early degassing and mantle evolution, as the I–Xe and Pu–Xe systems are sensitive to the first ~100 Ma and 500 Ma of Earth history, respectively. In contrast, the U–Xe system evolves throughout Earth history. Given the limited number of Xe isotopic observations from 7°E and the Oblique Supersegment, here we discuss only Xe data from the Orthogonal Supersegment. Depleted MORBs from the Equatorial Atlantic (Tucker et al., 2012), N. Atlantic popping rock 2ΠD43 (Moreira et al., 1998; Kunz et al., 1998) and Icelandic basalt DICE (Mukhopadhyay, 2012) are included for comparison.

We present the Xe data in two different Xe isotopic spaces: $^{136}Xe/^{130}Xe$ vs. $^{129}Xe/^{130}Xe$ (Fig. 8) and error-weighted averages in $^{129}Xe/^{136}Xe$ vs. $^{130}Xe/^{136}Xe$ (Fig. 9). In $^{136}Xe/^{130}Xe$ vs. $^{129}Xe/^{130}Xe$ space, individual step-crushes define a linear trend (Fig. 8) that reflects two-component mixing between the mantle source and atmosphere. The slope of the line is inversely proportional to $^{129}Xe/^{136}Xe$ in the mantle source and reflects the mantle source degassing history. For example, a mantle reservoir that undergoes degassing after I and Pu are extinct will have low concentrations of primordial ^{130}Xe, radiogenic ^{129}Xe and fissiogenic ^{136}Xe produced by extinct ^{244}Pu. Addition of ^{136}Xe from ^{238}U fission to such a degassed source would not change the $^{129}Xe/^{130}Xe$ ratio of the reservoir, but would increase the $^{136}Xe/^{130}Xe$ ratio. Therefore, a steeper slope in $^{136}Xe/^{130}Xe$ vs.

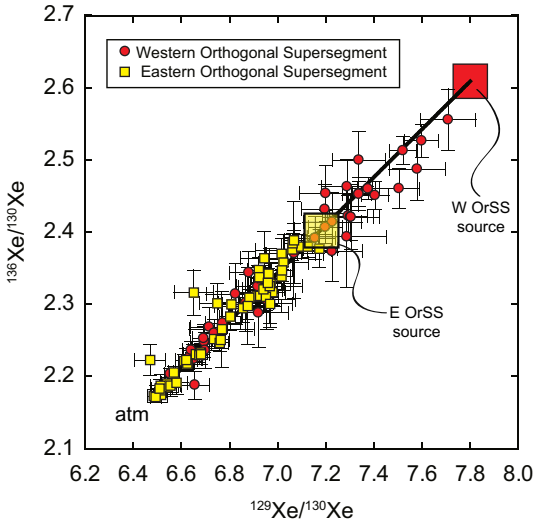

Fig. 8. SWIR Xe isotope systematics in $^{136}Xe/^{130}Xe$ vs. $^{129}Xe/^{130}Xe$ space for Orthogonal Supersegment samples. Step-crushing generates a well-defined linear mixing array between air and the mantle source (approximate source $^{129}Xe/^{130}Xe$ from Ar–Xe extrapolations; Fig. 4). The extrapolated source $^{129}Xe/^{130}Xe$ values (indicated by large squares) are significantly lower at the eastern Orthogonal Supersegment than the western Orthogonal Supersegment, and may reflect recycling of atmospheric Xe.

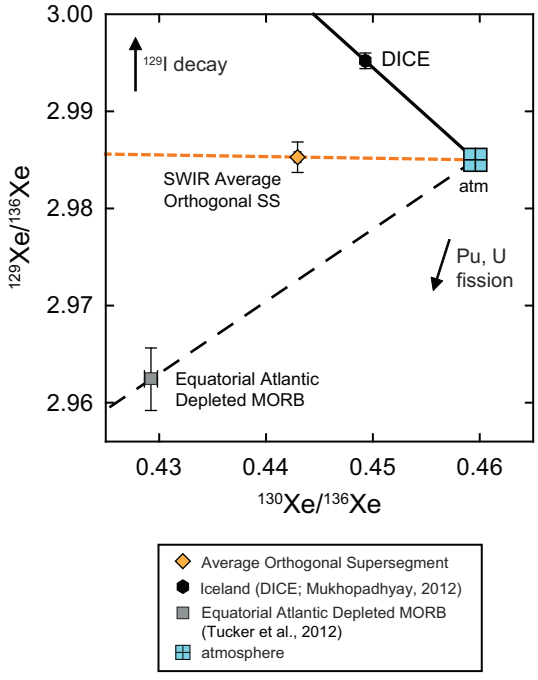

Fig. 9. Error-weighted averages of measured $^{129}Xe/^{136}Xe$ plotted against error-weighted averages of measured $^{130}Xe/^{136}Xe$ for the SWIR Orthogonal Supersegment. Data from Iceland (DICE; Mukhopadhyay, 2012) and depleted Equatorial Atlantic MORB (Tucker et al., 2012) are shown for comparison. N. Atlantic popping rock 2ΠD43 is not shown in this figure since $^{129}Xe/^{136}Xe$ ratios are not directly available (Moreira et al., 1998). An advantage of the $^{130}Xe/^{136}Xe$ vs. $^{129}Xe/^{136}Xe$ plot over the $^{129}Xe/^{130}Xe$ vs. $^{136}Xe/^{130}Xe$ representation is that the *x* and *y* errors are not as strongly correlated as in Fig. 8. The atmospheric composition is indicated along with vectors representing ^{129}I decay and (Pu+U) fission. Mixing in this space is linear and lines representing two-component mixing between the measured composition and atmosphere are indicated. The weighted average of the measured $^{129}Xe/^{136}Xe$ ratio in the SWIR Orthogonal Supersegment is demonstrably distinct from the weighted average of DICE and the depleted Equatorial Atlantic MORB samples.

$^{129}Xe/^{130}Xe$ space indicates a relatively degassed source. Likewise, in $^{129}Xe/^{136}Xe$ vs. $^{130}Xe/^{136}Xe$ space (Fig. 9), a degassed source should have low $^{129}Xe/^{136}Xe$ and $^{130}Xe/^{136}Xe$, since ^{130}Xe is primordial and production of ^{129}Xe stops after the first 100 Ma of Earth history.

Fig. 8 shows the linear array defined by the SWIR Orthogonal Supersegment data in $^{136}Xe/^{130}Xe$ vs. $^{129}Xe/^{130}Xe$ space. The least-squares best fit slope of 0.331 ± 0.006 is statistically indistinguishable from the 2ΠD43 slope of 0.324 ± 0.006 (Moreira et al., 1998; Kunz et al., 1998). However, the SWIR slope is shallower than the slope of 0.375 ± 0.009 for the depleted Equatorial Atlantic MORBs (Tucker et al., 2012) and steeper than the slope of 0.306 ± 0.01 for Iceland (Mukhopadhyay, 2012). Likewise, the error-weighted average $^{129}Xe/^{136}Xe$ ratio ($n=86$; Fig. 9) from the Orthogonal Supersegment is intermediate to Iceland (DICE; Mukhopadhyay, 2012) and the depleted Equatorial Atlantic MORBs (Tucker et al., 2012) and well-resolved from both. Since the SWIR, DICE and Equatorial Atlantic samples were all analyzed using the same procedure in the same laboratory, the differences between these three groups of basalts are not related to measurement artifacts. Instead, the differences must reflect different degrees of degassing of the mantle sources: the depleted Equatorial Atlantic MORB source is most degassed; the SWIR Orthogonal Supersegment MORB source is slightly less degassed, and the Iceland source is least degassed. Hence, the depleted MORBs from the Equatorial Atlantic and the MORBs from the SWIR Orthogonal Supersegment indicate that there are small variations in $^{129}Xe/^{136}Xe$ even in regions removed from obvious influence of mantle plumes (Fig. 9).

Mukhopadhyay (2012) argued that the Iceland and N. Atlantic popping rock mantle sources are distinct in $^{129}Xe/^{136}Xe$–$^{130}Xe/^{136}Xe$ space and that the two sources cannot be related by preferential recycling of atmospheric heavy noble gases (cf., Holland and Ballentine, 2006) or by addition of fission-produced ^{136}Xe into the Iceland source. The new observations from the SWIR Orthogonal Supersegment provide conclusive evidence for this distinction in Xe isotopic composition between MORBs and Iceland (Fig. 9). Sources related by recycling of atmospheric Xe would be collinear with the atmospheric composition; the Iceland and SWIR mantle Xe compositions are clearly not collinear. We note that recycling of atmospheric volatiles to the deep Earth may occur, but we emphasize that differential recycling by itself cannot explain the Xe isotopic difference between MORBs and Iceland. Therefore, early separation of the reservoir supplying noble gases to the Iceland plume from the MORB source and a lower degree of degassing for the Iceland source are the only viable explanations for the differences between the Iceland plume and MORB heavy noble gas isotopic compositions (Mukhopadhyay, 2012). However, the persistence of mantle reservoirs created very early in Earth history does not necessarily imply convective isolation; rather, the two reservoirs may have been processed at different rates and have experienced limited direct mixing over Earth history (Gonnermann and Mukhopadhyay, 2009).

6. Conclusions

We present high-precision Ne, Ar and Xe isotopic compositions, and He, CO_2, Ne, Ar and Xe abundances measured in basalt glasses from the SWIR between 7°E and 25°E. We find systematic and significant variations in He, Ne, Ar and Xe isotopic compositions across the study area. Basalts with low $^4He/^3He$ are found to be characterized by low source $^{21}Ne/^{22}Ne_{(E)}$, low $^{40}Ar/^{36}Ar_{(E)}$, and intermediate $^{129}Xe/^{130}Xe_{(E)}$, indicating the influence of a less-degassed reservoir in the mantle source at 7°E. In contrast, basalts with higher $^4He/^3He$ are characterized by higher $^{21}Ne/^{22}Ne_{(E)}$, $^{40}Ar/^{36}Ar_{(E)}$, and $^{129}Xe/^{130}Xe_{(E)}$, indicating a comparatively degassed mantle source (Figs. 6 and 7). However, among MORBs removed from the influence of any known hotspot, we find significant variations in $^{40}Ar/^{36}Ar_{(E)}$ and $^{129}Xe/^{130}Xe_{(E)}$ over a limited range of $^4He/^3He$ and $^{21}Ne/^{22}Ne_{(E)}$ compositions (Figs. 6 and 7), indicating source heterogeneity in Ar and Xe isotopes. The difference in $^{40}Ar/^{36}Ar_{(E)}$ and $^{129}Xe/^{130}Xe_{(E)}$ between the western and eastern Orthogonal Supersegment reflects sampling of distinct mantle domains, and suggests that the Dupal mantle is characterized by low $^{40}Ar/^{36}Ar_{(E)}$ and $^{129}Xe/^{130}Xe_{(E)}$ relative to N. Atlantic and Pacific MORB mantle sources. Low $^{129}Xe/^{130}Xe_{(E)}$ in the Dupal mantle would indicate that Dupal cannot represent unmodified delaminated SCLM unless the SCLM is very ancient (>4.45 Ga). If SCLM is younger, it must have been metasomatized by subduction zone fluids carrying recycled atmospheric Ar and Xe.

High-precision Xe isotopic measurements allow us to demonstrate that SWIR MORB $^{129}Xe/^{136}Xe$–$^{130}Xe/^{136}Xe$ systematics cannot be related to OIB systematics solely through recycling of atmospheric noble gases (Figs. 8 and 9). Therefore, a lower degree of degassing for the plume source and limited mixing between plume and MORB sources over 4.45 Ga remain the viable explanation for observed differences in MORB and OIB heavy noble gas compositions.

Acknowledgments

We thank Dr. Shichun Huang and Dr. Allison Gale for comments and discussions. Constructive comments from Dr. Philippe Sarda and two anonymous reviewers helped to improve the manuscript. This work was supported by NSF Grant No. OCE 0929193.

Appendix A. Supporting information

Supplementary data associated with this article can be found in the online version at http://dx.doi.org/10.1016/j.epsl.2012.10.017.

References

Allègre, C.J., Staudacher, T., Sarda, P., 1987. Rare-gas systematics—formation of the atmosphere, evolution and structure of the earth's mantle. Earth Planet. Sci. Lett. 81, 127–150.

Ballentine, C.J., Barfod, D.N., 2000. The origin of air-like noble gases in MORB and OIB. Earth Planet. Sci. Lett. 180, 39–48, http://dx.doi.org/10.1016/s0012-821x(00)00161-8.

Ballentine, C.J., Holland, G., 2008. What CO_2 well gases tell us about the origin of noble gases in the mantle and their relationship to the atmosphere. Philos. Trans. R. Soc. A 366, 4183–4203, http://dx.doi.org/10.1098/rsta.2008.0150.

Burnard, P., 1999. Origin of argon–lead isotopic correlation in basalts. Science 286, 871.

Caffee, M.W., Hudson, G.U., Velsko, C., Huss, G.R., Alexander, E.C., Chivas, A.R., 1999. Primordial noble gases from Earth's mantle: identification of a primitive volatile component. Science 285, 2115–2118.

Dasgupta, R., Hirschmann, M.M., Withers, A.C., 2004. Deep global cycling of carbon constrained by the solidus of anhydrous, carbonated eclogite under upper mantle conditions. Earth Planet. Sci. Lett. 227, 73–85, http://dx.doi.org/10.1016/j.epsl.2004.08.004.

Davies, G.F., 2010. Noble gases in the dynamic mantle. Geochem. Geophys. Geosyst. 11, Q03005, http://dx.doi.org/10.1029/2009gc002801.

Dick, H.J.B., Lin, J., Schouten, H., 2003. An ultraslow-spreading class of ocean ridge. Nature 426, 405–412, http://dx.doi.org/10.1038/nature02128.

Douglass, J., Schilling, J.G., Fontignie, D., 1999. Plume-ridge interactions of the Discovery and Shona mantle plumes with the southern mid-Atlantic ridge (40 degrees-55 degrees S). J. Geophys. Res.: Solid Earth 104, 2941–2962.

Dupre, B., Allegre, C.J., 1983. Pb–Sr isotope variation in Indian Ocean basalts and mixing phenomena. Nature 303, 142–146.

Furi, E., Hilton, D.R., Halldorsson, S.A., Barry, P.H., Hahm, D., Fischer, T.P., Gronvold, K., 2010. Apparent decoupling of the He and Ne isotope systematics of the Icelandic

mantle: the role of He depletion, melt mixing, degassing fractionation and air interaction. Geochim. Cosmochim. Acta 74, 3307–3332.
Gautheron, C., Moreira, M., Allegre, C., 2005. He, Ne and Ar composition of the European lithospheric mantle. Chem. Geol. 217, 97–112, http://dx.doi.org/10.1016/j.chemgeo.2004.12.009.
Georgen, J.E., Kurz, M.D., Dick, H.J.B., Lin, J., 2003. Low $^{3}He/^{4}He$ ratios in basalt glasses from the western Southwest Indian Ridge (10°–24°e). Earth Planet. Sci. Lett. 206, 509–528, http://dx.doi.org/10.1016/s0012-821x(02)01106-8.
Gonnermann, H.M., Mukhopadhyay, S., 2009. Preserving noble gases in a convecting mantle. Nature 459, U560–U588, http://dx.doi.org/10.1038/nature08018.
Graham, D.W., 2002. Noble gas isotope geochemistry of mid-ocean ridge and ocean island basalts: characterization of mantle source reservoirs. In: Porcelli, D., Ballentine, C.J., Wieler, R. (Eds.), Noble Gases in Geochemistry and Cosmochemistry, Reviews in Mineralogy and Geochemistry, vol. 47. Mineralogical Society of America and Geochemical Society, Washington, DC, pp. 247–317.
Graham, D.W., Humphris, S.E., Jenkins, W.J., Kurz, M.D., 1992. Helium isotope geochemistry of some volcanic rocks from Saint-Helena. Earth Planet. Sci. Lett. 110, 121–131.
Graham, D.W., Lupton, J.E., Spera, F.J., Christie, D.M., 2001. Upper-mantle dynamics revealed by helium isotope variations along the Southeast Indian ridge. Nature 409, 701–703.
Hanyu, T., Dunai, T.J., Davies, G.R., Kaneoka, I., Nohda, S., Uto, K., 2001. Noble gas study of the Reunion hotspot: evidence for distinct less-degassed mantle sources. Earth Planet. Sci. Lett. 193, 83–98.
Hanyu, T., Kaneoka, I., 1998. Open system behavior of helium in case of the HIMU source area. Geophys. Res. Lett. 25, 687–690.
Hanyu, T., Kaneoka, I., Nagao, K., 1999. Noble gas study of HIMU and EM ocean island basalts in the Polynesian region. Geochim. Cosmochim. Acta 63, 1181–1201.
Harrison, D., Burnard, P., Turner, G., 1999. Noble gas behaviour and composition in the mantle: constraints from the Iceland plume. Earth Planet. Sci. Lett. 171, 199–207.
Hart, S.R., 1984. A large-scale isotope anomaly in the southern-hemisphere mantle. Nature 309, 753–757.
Hart, S.R., Hauri, E.H., Oschmann, L.A., Whitehead, J.A., 1992. Mantle plumes and entrainment—isotopic evidence. Science 256, 517–520.
Hawkesworth, C.J., Mantovani, M.S.M., Taylor, P.N., Palacz, Z., 1986. Evidence from the Parana of South Brazil for a continental contribution to Dupal basalts. Nature 322, 356–359.
Hilton, D.R., Macpherson, C.G., Elliott, T.R., 2000. Helium isotope ratios in mafic phenocrysts and geothermal fluids from La Palma, the Canary Islands (Spain): implications for HIMU mantle sources. Geochim. Cosmochim. Acta 64, 2119–2132.
Holland, G., Ballentine, C.J., 2006. Seawater subduction controls the heavy noble gas composition of the mantle. Nature 441, 186–191, http://dx.doi.org/10.1038/Nature04761.
Honda, M., Mcdougall, I., 1998. Primordial helium and neon in the earth—a speculation on early degassing. Geophys. Res. Lett. 25, 1951–1954.
Honda, M., Woodhead, J.D., 2005. A primordial solar-neon enriched component in the source of EM-I-type ocean island basalts from the Pitcairn seamounts, Polynesia. Earth Planet. Sci. Lett. 236, 597–612, http://dx.doi.org/10.1016/j.epsl.2005.05.038.
Huang, S.C., Farkas, J., Jacobsen, S.B., 2011. Stable calcium isotopic compositions of Hawaiian shield lavas: evidence for recycling of ancient marine carbonates into the mantle. Geochim. Cosmochim. Acta 75, 4987–4997, http://dx.doi.org/10.1016/j.gca.2011.06.010.
Kendrick, M.A., Scambelluri, M., Honda, M., Phillips, D., 2011. High abundances of noble gas and chlorine delivered to the mantle by serpentinite subduction. Nat. Geosci. 4, 807–812, http://dx.doi.org/10.1038/Ngeo1270.
Kunz, J., Staudacher, T., Allegre, C.J., 1998. Plutonium-fission xenon found in Earth's mantle. Science 280, 877–880.
Kurz, M.D., Jenkins, W.J., Schilling, J.G., Hart, S.R., 1982. Helium isotopic variations in the mantle beneath the Central-North Atlantic ocean. Earth Planet. Sci. Lett. 58, 1–14.
Kurz, M.D., Le Roex, A.P., Dick, H.J.B., 1998. Isotope geochemistry of the oceanic mantle near the Bouvet triple junction. Geochim. Cosmochim. Acta 62, 841–852.
Kurz, M.D., Moreira, M., Curtice, J., Lott, D.E., Mahoney, J.J., Sinton, J.M., 2005. Correlated helium, neon, and melt production on the super-fast spreading East Pacific Rise near 17°S. Earth Planet. Sci. Lett. 232, 125–142, http://dx.doi.org/10.1016/j.epsl.2005.01.005.
Le Roex, A.P., Dick, H.J.B., Watkins, R.T., 1992. Petrogenesis of anomalous K-enriched MORB from the Southwest Indian Ridge—11°53'E to 14°38'E. Contrib. Mineral. Petrol. 110, 253–268.
Madureira, P., Moreira, M., Mata, J., Allegre, C.J., 2005. Primitive neon isotopes in Terceira Island (Azores archipelago). Earth Planet. Sci. Lett. 233, 429–440, http://dx.doi.org/10.1016/j.epsl.2005.02.030.
Mahoney, J., Leroex, A.P., Peng, Z., Fisher, R.L., Natland, J.H., 1992. Southwestern limits of Indian-Ocean ridge mantle and the origin of low $^{206}Pb/^{204}Pb$ mid-ocean ridge basalt—isotope systematics of the central Southwest Indian Ridge (17°E–50°E). J. Geophys. Res.: Solid Earth 97, 19771–19790.
Mahoney, J.J., Natland, J.H., White, W.M., Poreda, R., Bloomer, S.H., Fisher, R.L., Baxter, A.N., 1989. Isotopic and geochemical provinces of the western Indian-Ocean spreading centers. J. Geophys. Res.: Solid Earth 94, 4033–4052.
Marty, B., Tolstikhin, I.N., 1998. CO_2 fluxes from mid-ocean ridges, arcs and plumes. Chem. Geol. 145, 233–248.
Marty, B., Sano, Y., France-Lanord, C., 2001. Water-saturated oceanic lavas from the Manus Basin: volatile behaviour during assimilation-fractional crystallisation-degassing (AFCD). J. Volcanol. Geotherm. Res. 108, 1–10.
Matsumoto, T., Chen, Y.L., Matsuda, J., 2001. Concomitant occurrence of primordial and recycled noble gases in the Earth's mantle. Earth Planet. Sci. Lett. 185, 35–47.
Moreira, M., Staudacher, T., Sarda, P., Schilling, J.G., Allegre, C.J., 1995. A primitive plume neon component in MORB—the Shona Ridge anomaly, South-Atlantic (51–52°S). Earth Planet. Sci. Lett. 133, 367–377.
Moreira, M., Kunz, J., Allegre, C., 1998. Rare gas systematics in popping rock: isotopic and elemental compositions in the upper mantle. Science 279, 1178–1181.
Moreira, M., Doucelance, R., Kurz, M.D., Dupre, B., Allegre, C.J., 1999. Helium and lead isotope geochemistry of the Azores archipelago. Earth Planet. Sci. Lett. 169, 189–205.
Moreira, M., Escartin, J., Gayer, E., Hamelin, C., Bezos, A., Guillon, F., Cannat, M., 2011. Rare gas systematics on Lucky Strike basalts (37°N, North Atlantic): evidence for efficient homogenization in a long-lived magma chamber system? Geophys. Res. Lett. 38, L08304, http://dx.doi.org/10.1029/2011gl046794.
Mukhopadhyay, S., 2012. Early differentiation and volatile accretion recorded in deep-mantle neon and xenon. Nature 486, 101–104, http://dx.doi.org/10.1038/Nature11141.
O'Nions, R.K., Tolstikhin, I.N., 1996. Limits on the mass flux between lower and upper mantle and stability of layering. Earth Planet. Sci. Lett. 139, 213–222.
Parai, R., Mukhopadhyay, S., Lassiter, J.C., 2009. New constraints on the HIMU mantle from neon and helium isotopic compositions of basalts from the Cook-Austral Islands. Earth Planet. Sci. Lett. 277, 253–261, http://dx.doi.org/10.1016/j.epsl.2008.10.014.
Pepin, R.O., Porcelli, D., 2002. Origin of noble gases in the terrestrial planets. In: Porcelli, D., Ballentine, C.J., Wieler, R. (Eds.), Noble Gases in Geochemistry and Cosmochemistry. In: Reviews in Mineralogy and Geochemistry, vol. 47. Mineralogical Society of America and Geochemical Society, Washington, DC, pp. 191–246.
Phinney, D., Tennyson, J., Frick, U., 1978. Xenon in CO_2 well gas revisited. J. Geophys. Res. 83, 2313–2319.
Porcelli, D., Wasserburg, G.J., 1995. Mass-transfer of helium, neon, argon, and xenon through a steady-state upper-mantle. Geochim. Cosmochim. Acta 59, 4921–4937.
Press, W.H., Teukolsky, S.A., Vetterling, W.T., Flannery, B.P., 1992. Numerical Recipes in C: The Art of Scientific Computing, second edition Cambridge University Press, New York.
Raquin, A., Moreira, M.A., Guillon, F., 2008. He, Ne and Ar systematics in single vesicles: mantle isotopic ratios and origin of the air component in basaltic glasses. Earth Planet. Sci. Lett. 274, 142–150, http://dx.doi.org/10.1016/j.epsl.2008.07.007.
Sarda, P., Moreira, M., Staudacher, T., 1999. Argon–lead isotopic correlation in Mid-Atlantic Ridge basalts. Science 283, 666–668.
Sarda, P., Moreira, M., Staudacher, T., Schilling, J.G., Allegre, C.J., 2000. Rare gas systematics on the southernmost Mid-Atlantic Ridge: constraints on the lower mantle and the Dupal source. J. Geophys. Res.: Solid Earth 105, 5973–5996.
Sarda, P., Staudacher, T., Allegre, C.J., 1985. $^{40}Ar/^{36}Ar$ in MORB glasses—constraints on atmosphere and mantle evolution. Earth Planet. Sci. Lett. 72, 357–375.
Shaw, A.M., Hilton, D.R., Macpherson, C.G., Sinton, J.M., 2001. Nucleogenic neon in high $^{3}He/^{4}He$ lavas from the Manus back-arc basin: a new perspective on He–Ne decoupling. Earth Planet. Sci. Lett. 194, 53–66.
Standish, J.J., 2006. The Influence of Ridge Geometry at the Ultraslow-Spreading Southwest Indian Ridge (9–25°E): Basalt Composition Sensitivity to Variations in Source and Process. Ph.D. Thesis. MIT WHOI Joint Program in Oceanography/Applied Ocean Science and Engineering.
Standish, J.J., Dick, H.J.B., Michael, P.J., Melson, W.G., O'Hearn, T., 2008. MORB generation beneath the ultraslow spreading Southwest Indian Ridge (9–25°E): major element chemistry and the importance of process versus source. Geochem. Geophys. Geosyst. 9, Q05004, http://dx.doi.org/10.1029/2008gc001959.
Staudacher, T., 1987. Upper mantle origin for Harding County well gases. Nature 325, 605–607.
Staudacher, T., Allegre, C.J., 1982. Terrestrial xenology. Earth Planet. Sci. Lett. 60, 389–406.
Staudacher, T., Sarda, P., Richardson, S.H., Allegre, C.J., Sagna, I., Dmitriev, L.V., 1989. Noble gases in basalt glasses from a Mid-atlantic Ridge topographic high at 14°N—geodynamic consequences. Earth Planet. Sci. Lett. 96, 119–133.
Storey, M., Saunders, A.D., Tarney, J., Gibson, I.L., Norry, M.J., Thirlwall, M.F., Leat, P., Thompson, R.N., Menzies, M.A., 1989. Contamination of Indian-Ocean asthenosphere by the Kerguelen-Heard mantle plume. Nature 338, 574–576.
Stuart, F.M., Lass-Evans, S., Fitton, J.G., Ellam, R.M., 2003. High $^{3}He/^{4}He$ ratios in picritic basalts from Baffin Island and the role of a mixed reservoir in mantle plumes. Nature 424, 57–59.
Sumino, H., Burgess, R., Mizukami, T., Wallis, S.R., Holland, G., Ballentine, C.J., 2010. Seawater-derived noble gases and halogens preserved in exhumed mantle

wedge peridotite. Earth Planet. Sci. Lett. 294, 163–172, http://dx.doi.org/10.1016/j.epsl.2010.03.029.
Tolstikhin, I.N., Marty, B., 1998. The evolution of terrestrial volatiles: a view from helium, neon, argon and nitrogen isotope modeling. Chem. Geol. 147, 27–52.
Trieloff, M., Kunz, J., Clague, D.A., Harrison, D., Allegre, C.J., 2000. The nature of pristine noble gases in mantle plumes. Science 288, 1036–1038.
Tucker, J.M., Mukhopadhyay, S., Schilling, J.G., 2012. The heavy noble gas composition of the depleted MORB mantle (DMM) and its implications for the origin of heterogeneities in the upper mantle. Earth Planet. Sci. Lett. 355–356, 244–254. http://dx.doi.org/10.1016/j.epsl.2012.08.025.
Wetherill, G.W., 1954. Variations in the isotopic abundances of neon and argon extracted from radioactive minerals. Phys. Rev. 96, 679–683.
Yamamoto, J., Kaneoka, I., Nakai, S., Kagi, H., Prikhod'ko, V.S., Arai, S., 2004. Evidence for subduction-related components in the subcontinental mantle from low $^{3}He/^{4}He$ and $^{40}Ar/^{36}Ar$ ratio in mantle xenoliths from Far Eastern Russia. Chem. Geol. 207, 237–259, http://dx.doi.org/10.1016/j.chemgeo.2004.03.007.
Yatsevich, I., Honda, M., 1997. Production of nucleogenic neon in the Earth from natural radioactive decay. J. Geophys. Res.: Solid Earth 102, 10291–10298.
Yokochi, R., Marty, B., 2004. A determination of the neon isotopic composition of the deep mantle. Earth Planet. Sci. Lett. 225, 77–88, http://dx.doi.org/10.1016/j.espl.2004.06.010.
York, D., 1969. Least squares fitting of a straight line with correlated errors. Earth Planet. Sci. Lett. 5, 320–324.
Zindler, A., Hart, S., 1986. Chemical geodynamics. Annu. Rev. Earth Planet. Sci. 14, 493–571.
Zindler, A., Jagoutz, E., Goldstein, S., 1982. Nd, Sr and Pb isotopic systematics in a 3-component mantle—a new perspective. Nature 298, 519–523.